Geoscience Frontiers 6 (2015) 793–805

HOSTED BY

Contents lists available at ScienceDirect

China University of Geosciences (Beijing)

Geoscience Frontiers

journal homepage: www.elsevier.com/locate/gsf

Research paper

Damage and geological assessment of the 18 September 2011 M_w 6.9 earthquake in Sikkim, India using very high resolution satellite data

Tapas R. Martha*, K. Babu Govindharaj, K. Vinod Kumar

National Remote Sensing Centre (NRSC), Indian Space Research Organisation (ISRO), Hyderabad 500 037, India

ARTICLE INFO

Article history:
Received 19 July 2013
Received in revised form
13 December 2013
Accepted 30 December 2013
Available online 26 February 2014

Keywords:
International Charter
Damage
Landslide
Fault
VHR
Disaster

ABSTRACT

Post-disaster very high resolution (VHR) satellite data are potential sources to provide detailed information on damage and geological changes for a large area in a short time. In this paper, we studied landslides triggered by the M_w 6.9 earthquake in Sikkim, India which occurred on 18 September 2011 using VHR data from Cartosat-1, GeoEye-1, QuickBird-2 and WorldView-2 satellites. Since the earthquake-affected area is located in mostly inaccessible Himalayan terrain, VHR data from these satellites provided a unique opportunity for quick and synoptic assessment of the damage. Using visual change analysis technique through comparison of pre- and post-earthquake images, we assessed the damage caused by the event. A total of 123 images acquired from eight satellites, covering an area of 4105 km^2 were analysed and 1196 new landslides triggered by the earthquake were mapped. Road blockages and severely affected villages were also identified. Geological assessment of the terrain highlighted linear disposition of landslides along existing fault scarps, suggesting a reactivation of fault. The landslide inventory map prepared from VHR images also showed a good correlation with the earthquake shake map. Results showed that several parts of north Sikkim, particularly Mangan and Chungthang, which are close to the epicentre, were severely affected by the earthquake, and that the event-based landslide inventory map can be used in future earthquake-triggered landslide susceptibility assessment studies.

1. Introduction

The Himalayas, which is an active fold-thrust belt, is prone to earthquakes. Recently, an earthquake of M_w 6.9 struck the India-Nepal border on 18 September 2011 at 06:10:48 PM (Indian Standard Time) with its epicentre located at 27.723°N and 88.064°E, and focus at 19.7 km depth (Source: United States Geological Survey (USGS)). The energy released by this shallow focus earthquake created tremors in far away regions lying in the plains of India, like many parts of Sikkim, West Bengal, Bihar, Jharkhand, Uttar Pradesh, Delhi (Mahajan et al., 2012). Adjoining areas in Nepal and China also witnessed this event. As per news reports several houses were damaged, 116 people were killed and many important roads were blocked by landslides in Sikkim.

In recent times, disaster support activities are becoming dependent on results derived from satellite data analysis (Tralli et al., 2005; Voigt et al., 2007). This is primarily due to the availability of a large number of Earth Observation Satellites, and better coordination among space-faring nations to share data in emergency scenarios. Indian Space Research Organisation (ISRO), as a part of its disaster management support activities, had programmed its satellites to acquire data over Sikkim area immediately after the earthquake. Subsequently, International Charter Space and Major Disasters (ICSMD) was also activated by ISRO to acquire data from other satellites over the earthquake-affected region.

Effective use of high resolution satellite data for rapid earthquake damage assessment has been shown comprehensively for three recent major earthquakes viz., Bam, Iran; Kashmir, India and Pakistan; and Wenchuan, China (Vinod Kumar et al., 2006; Arciniegas et al., 2007; Dunning et al., 2007; Gamba et al., 2007;

* Corresponding author. Tel.: +91 4023884276.
E-mail addresses: trmartha@rediffmail.com, tapas1977@gmail.com (T.R. Martha).
Peer-review under responsibility of China University of Geosciences (Beijing)

1674-9871/$ – see front matter © 2015, China University of Geosciences (Beijing) and Peking University. Production and hosting by Elsevier B.V. All rights reserved.
http://dx.doi.org/10.1016/j.gsf.2013.12.011

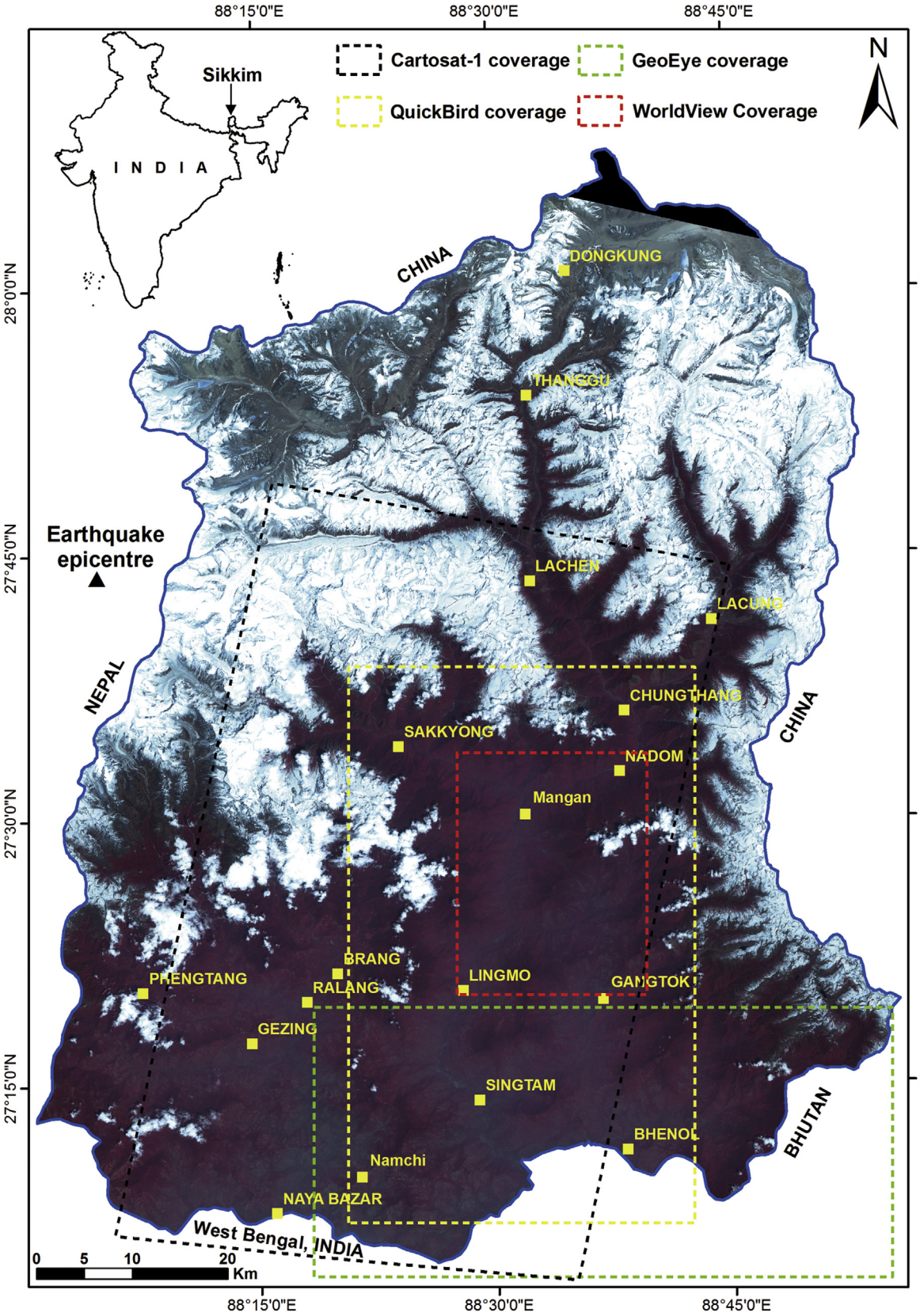

Figure 1. Pre-earthquake Resourcesat-2 LISS-III image (RGB = 432) showing synoptic view of Sikkim. Dashed lines indicate post-earthquake VHR data coverage.

Ray et al., 2009; Wang et al., 2009; Xu et al., 2013a). Vinod Kumar et al. (2006) showed how stereoscopic Cartosat-1 data were useful for damage assessment of the 2005 Kashmir earthquake. Remote sensing and GIS tools are also used for mapping and visualising tectonic elements such as faults in mountainous areas (Shen et al., 2011). Similarly, Lodhi (2013) highlighted the use of VHR images in the assessment of the 2010 Haiti earthquake. Voigt et al. (2007) stressed that since time is a constraint and fast extraction of damage maps is desirable after a disaster situation, sophisticated image processing techniques such as atmospheric corrections should only be used if it is absolutely necessary. However, damage maps should have high planimetric accuracy for which orthorectification of satellite images is required.

Apart from damage to houses, properties and infrastructures, earthquakes also trigger landslides (Jibson et al., 2006; Di et al., 2010; Lodhi, 2011; Xu et al., 2013b). Several studies have shown the effectiveness of satellite data to identify landslides triggered by earthquakes (Metternicht et al., 2005; Wang et al., 2009; Gorum et al., 2011; Stumpf and Kerle, 2011; Xu et al., 2013a). Large landslides triggered by earthquakes are also capable of creating temporary dams, which may create a potential situation for flash floods (Dunning et al., 2007).

The main objective of this study is to carry out a rapid assessment of the earthquake-affected Sikkim area using very high resolution (VHR) data acquired from different Earth Observation Satellites so that maps can be disseminated quickly for supporting disaster management activities. The assessment was mainly focused on identifying damage to roads, infrastructures, and demarcating landslides triggered after the earthquake. A geological assessment of the event was also performed to find out any possible reactivation of faults in this tectonically active area.

Table 1
Satellite data used in the Sikkim earthquake study.

Satellite	Date of acquisition	Sensor type (resolution)	Data type	No. of scenes	Source
Cartosat-1	05 October 2011	Panchromatic (2.5 m)	Stereoscopic	3	ISRO
	30 September 2011			3	
	22 March 2011			3	
GeoEye-1	05 October 2011	Panchromatic (38 cm) Multispectral (1.5 m)	Monoscopic	62	USGS
QuickBird-2	29 September 2011	Panchromatic (90 cm) Multispectral (2.8 m)	Monoscopic	18	USGS
WorldView-2	27 September 2011	Panchromatic (60 cm)	Monoscopic	8	USGS
WorldView-1	26 April 2011	Multispectral (2.4 m)		22	
Resourcesat-2 LISS-IV Mx	03 October 2011	Multispectral (5.8 m)	Monoscopic	1	ISRO
Resourcesat-2 LISS-III	13 March 2011	Multispectral (23.5 m)	Monoscopic	1	ISRO
Landsat-5 TM	12 September 2011	Multispectral (30 m)	Monoscopic	1	USGS
Landsat-7 ETM+	06 October 2011	Panchromatic (15 m) Multispectral (30 m)	Monoscopic	1	USGS

2. Materials and methods

2.1. Study area

A major part of Sikkim, India, covering an area of 4105 km^2, was investigated for assessing the damage caused by the earthquake (Fig. 1). This area is located in the high Himalayan terrain, where the occurrence of earthquakes and landslides is frequent (Kayal, 2001; Ghosh et al., 2010). Gangtok, the capital of the state of Sikkim, is a major city in this area. Kangchenjunga (8586 m), the third highest mountain peak of the world, is located in the study area. Major parts of north Sikkim are covered by snow and glaciers, and these are the source regions for many perennial rivers in the Indo-Gangetic plain. Tista is the major river in this area and is a tributary to the Brahmaputra river.

2.2. Geological setting

Geologically, Sikkim Himalaya is a seismically active area as the Indian plate is subducting under the Eurasian plate at approximately 50 mm/yr (Kayal, 2001; Kumar et al., 2007). The zones of subduction are represented on the surface as Indus Tsangpo Suture Zone (ITSZ). The Main Frontal Thrust (MFT), Main Boundary Thrust

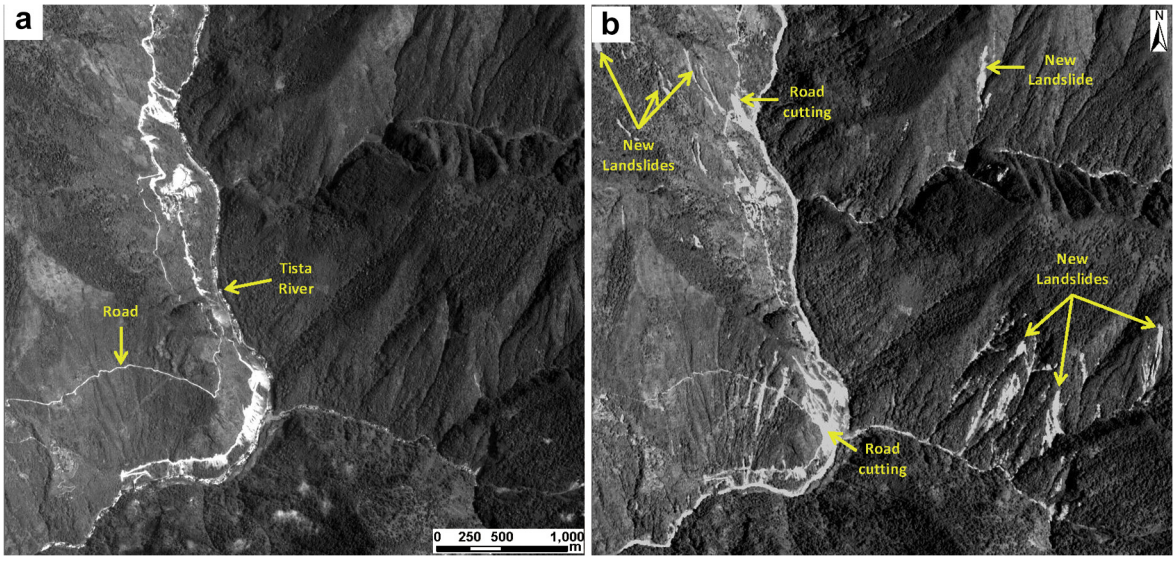

Figure 2. New landslides mapped from Cartosat-1 image in an area east of Mangan. (a) Pre-earthquake image, and (b) post-earthquake image. Road cuttings can be seen in both images.

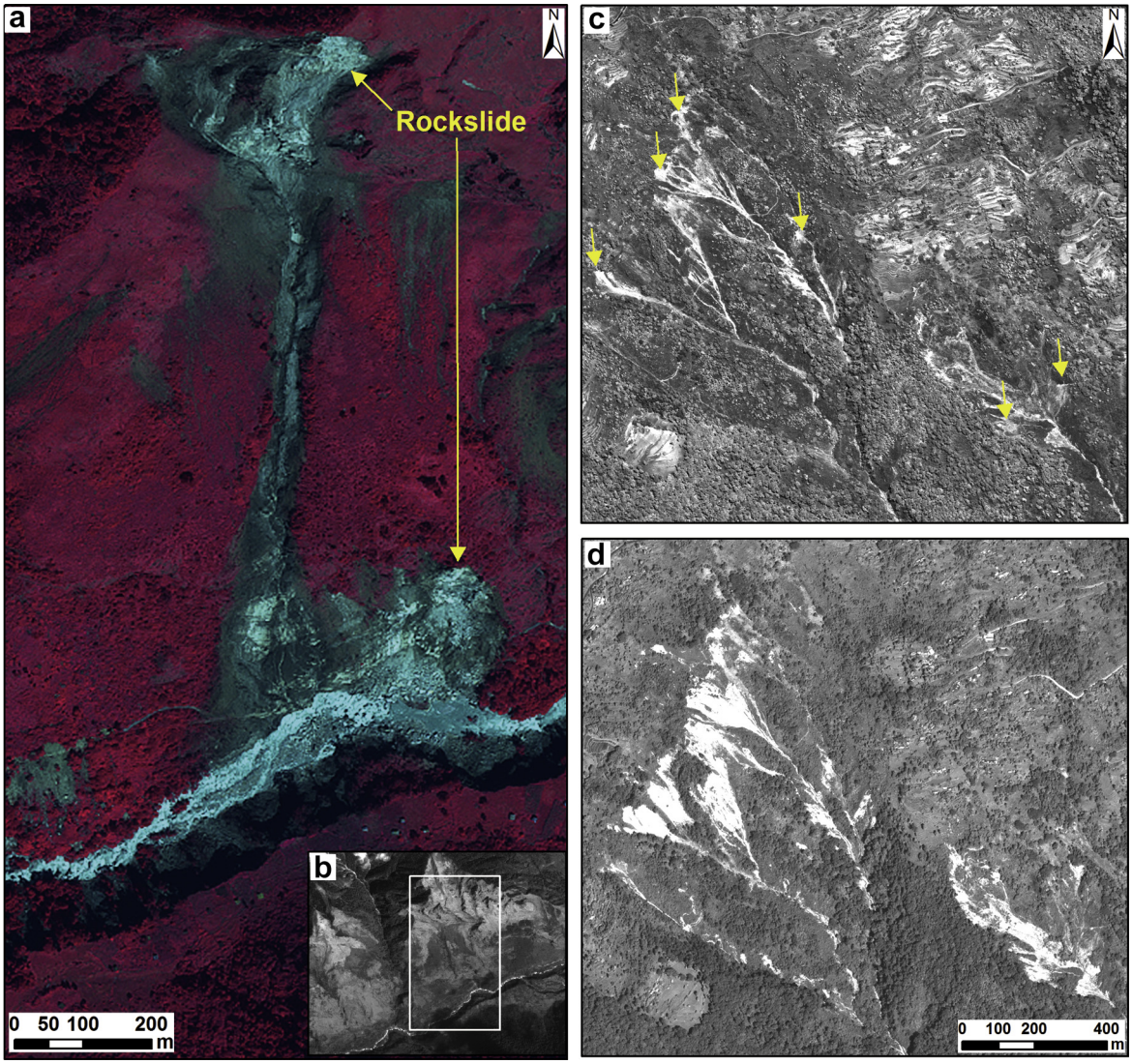

Figure 3. Different types of landslides triggered by the earthquake. (a) Post-earthquake WorldView-2 false colour composite (RGB = 432) of a large rock slide; (b) pre-earthquake Cartosat-1 image. Rectangle shows the location of WorldView-2 image; (c) old landslides (shown with arrow) as seen in the pre-earthquake WorldView-1 image; (d) reactivation of old landslides seen from post-earthquake GeoEye-1 image.

(MBT) and Main Central Thrust (MCT) are the other major tectonic features in the Himalayas developed subsequent to the subduction event (Kayal, 2001). MCT in Sikkim takes a convex turn to the north and also has a tectonic window known as Rangit window (Saha, 2013). While MBT separates low-grade lesser Himalayan rocks in the north from the Siwalik group of rocks in the south, MCT separates high-grade central crystalline rocks in the north from low-grade lesser Himalayan rocks in the south. In the Sikkim–Darjeeling Himalayas, most of the earthquake epicentres are located in regions between MBT and MCT (Kayal, 2001). The last time this area experienced a major earthquake (M_w 5.7) was on 14 February 2006.

2.3. Data sources

To assess damage caused by the earthquake, ISRO has programmed its satellites to acquire VHR images of Sikkim immediately after an event. Subsequently, on 19 September 2011, data were received from Cartosat-2 and Resourcesat-2. But, due to high cloud cover, these datasets could not be interpreted. To avoid the problem of clouds, microwave data from the Indian microwave satellite (RISAT-2) were acquired. Similarly, through an initiative of ICSMD, Radarsat-2 and TerraSAR-X data were provided by Canadian Space Agency and German Aerospace Centre, respectively. However, these microwave datasets could not be interpreted for damage assessment in this area due to: (i) unavailability of pre-earthquake microwave data with acquisition parameters similar to the post-earthquake data, and (ii) high geometric distortion due to foreshortening and layover effects, which is typical in steep terrains such as the Himalaya.

ISRO and other agencies of ICSMD continued their watch over Sikkim, and the first cloud-free VHR data for this area were available on 27 September 2011 from WorldView-2. On 30 September 2011, data for major part of the Sikkim were captured by Cartosat-1. A list of satellite data used for analysis of this event is provided in Table 1, and the extent of data coverage is shown in Fig. 1. Apart from VHR data, medium-resolution post-earthquake Landsat-7 ETM+ data were also analysed, particularly for those areas where there is a gap in the acquisition of VHR data. These datasets, although having few patches of cloud, were used for analysis since fast dissemination of results is a priority in any disaster situation. Several pre-earthquake images from the same satellites were also used during analysis (Table 1).

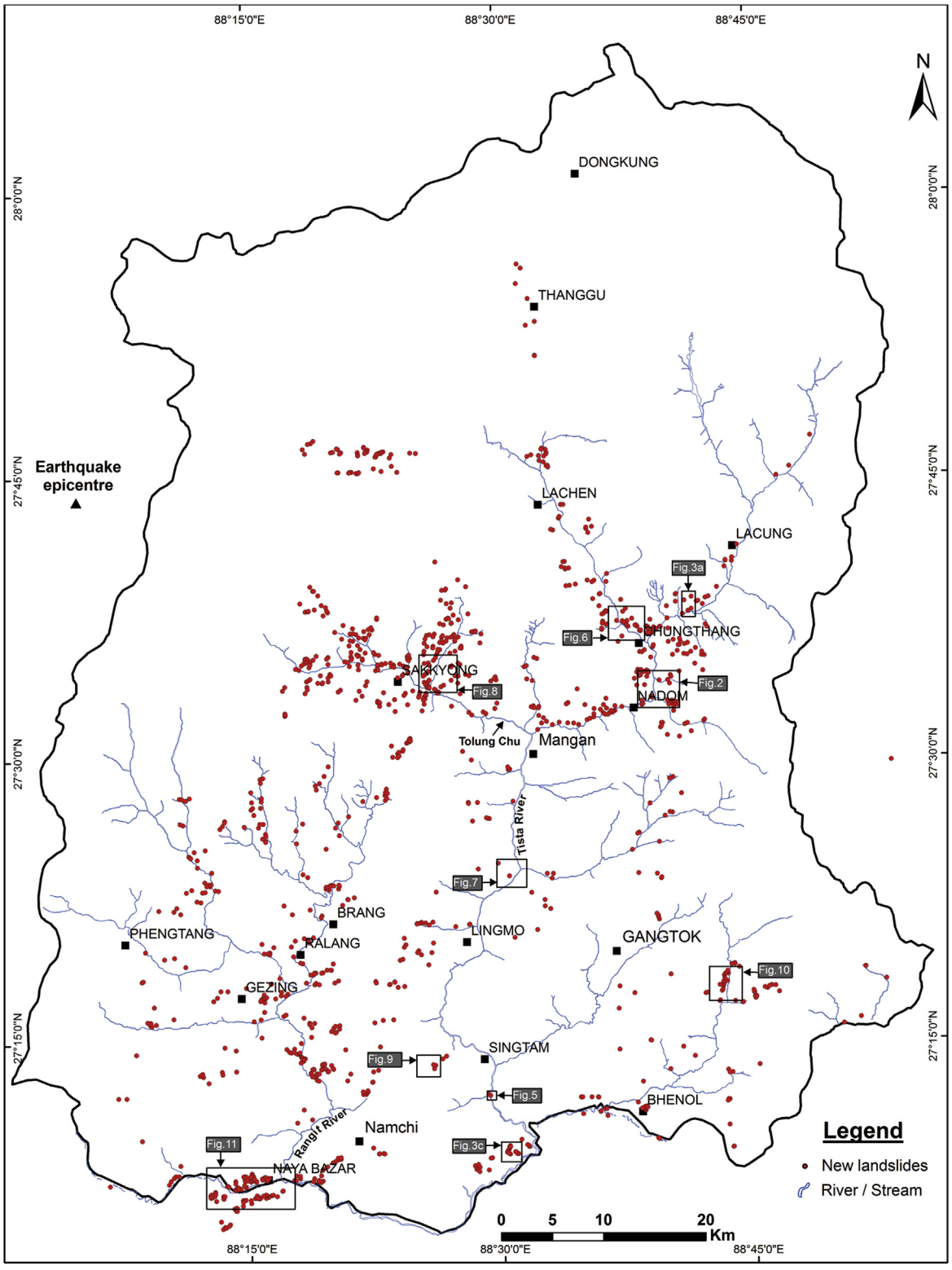

Figure 4. Post-earthquake landslide inventory created from VHR images. Landslide locations are marked as dots. Boxes identify the location of other figures shown in this paper.

2.4. Data processing

Firstly, stereoscopic Cartosat-1 data were processed for a 3D visualisation of the earthquake-affected area. Cartosat-1 has two panchromatic (PAN) cameras: PAN aft (−5°) and PAN fore (+26°), and are provided with rational polynomial coefficients (RPCs), which can be used for photogrammetric processing and subsequent generation of digital surface models (DSMs) and orthorectified images. High planimetric accuracy is desirable for products derived from satellite data for disaster support purposes (Voigt et al., 2007). In order to improve the planimetric accuracy of Cartosat-1 data, we used ground control points (GCPs) from the Indian national GCP

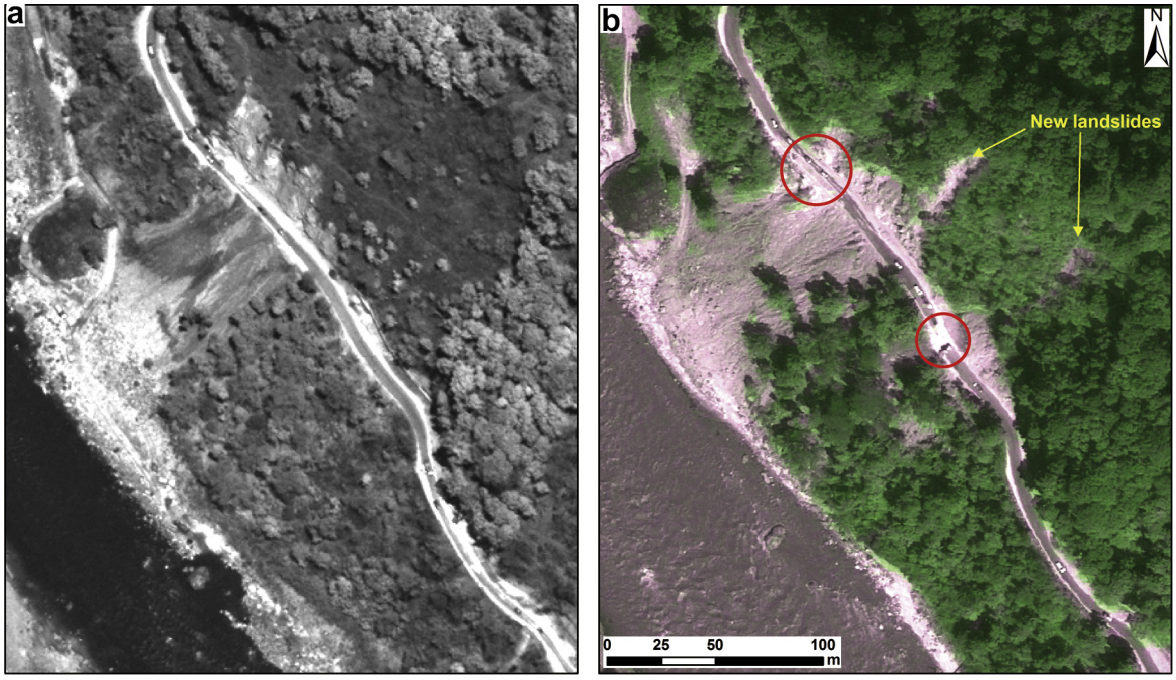

Figure 5. Blockage of road (highlighted with circles) adjacent to the Tista river due to landsliding. (a) Pre-earthquake WorldView-2 image, and (b) post-earthquake pansharpened GeoEye-1 image shown with natural colour composite.

library available with NRSC, which was created through a differential GPS (DGPS) survey. The stereo pairs were processed and block triangulation was performed using Leica Photogrammetric Suite (LPS) software. Subsequently, a 10 m DSM and Cartosat-1 orthorectified images were generated. GeoEye-1, QuickBird-2, WorldView-2 and Resourcesat-2 data were also orthorectified using a projective transform model with Cartosat-1 derived DSM. Uniform projection (UTM) and datum (WGS84) were maintained during the processing of pre- and post-earthquake Cartosat-1 data as well as other VHR datasets.

Pan-sharpening and contrast enhancement (e.g. standard deviation stretch) were the other data processing techniques attempted in this study for efficient visual change analysis. For example, pan-sharpening of the GeoEye-1 panchromatic image (38 cm) with its multispectral image (1.5 m) using Brovey transformation method resulted in a 38 cm (resolution) post-disaster colour image that provided detailed information about the damages.

2.5. Data analysis

A combination of panchromatic, multispectral, monoscopic and stereoscopic data was used for image interpretation. Visual change analysis by comparing post-earthquake images with the pre-earthquake images was mainly attempted to find earthquake-induced changes to the terrain. Stereoscopic interpretation of Cartosat-1 images was carried out using the Stereo Analyst module of the ERDAS software. Stereoscopic interpretation helped to appreciate the third dimension of the ground features (e.g.

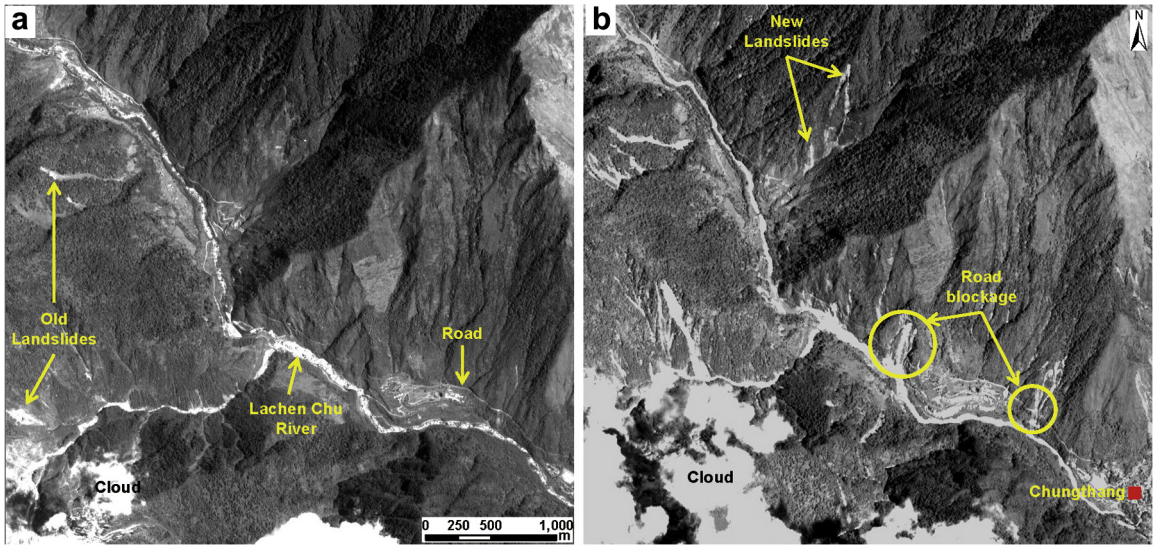

Figure 6. Parts of road completely destroyed by landslides triggered due to the earthquake near Chungthang area in north Sikkim. (a) pre-earthquake Cartosat-1 image, and (b) post-earthquake Cartosat-1 image.

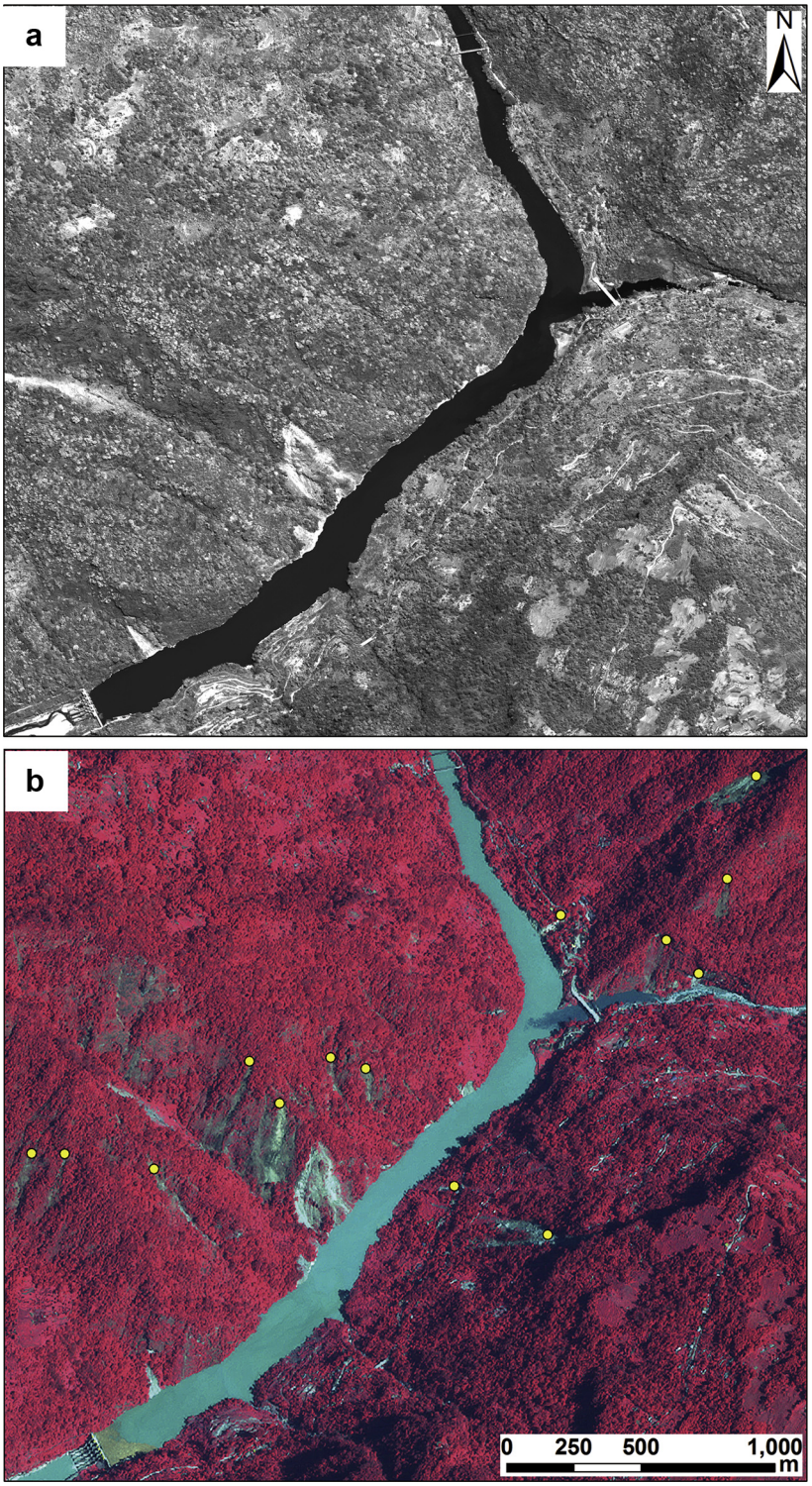

Figure 7. False colour composite (RGB = 432) of post-earthquake QuickBird-2 multispectral image (b) showing landslides in the reservoir area of a dam across Tista river. (a) Pre-earthquake panchromatic WorldView-1 image. High reflectance of water in the reservoir in the post-earthquake image is due to its sediment richness. New landslides triggered after the earthquake are shown with yellow dots.

building, bridge and landslide) and accurate identification of damaged objects. While Cartosat-1 was helpful for damage assessment due to the 3D visualisation of the terrain, GeoEye-1, WorldView-2 and QuickBird-2 data were able to provide details of the changes on the ground after the earthquake. The main goal of the image interpretation was to find out the damage to infrastructures (roads, bridges and dam sites), buildings, terrain (in the form of landsliding) and any other damages leading to economic losses.

3. Results

Details of the assessment and results derived from the analysis of VHR images are described in the following sections.

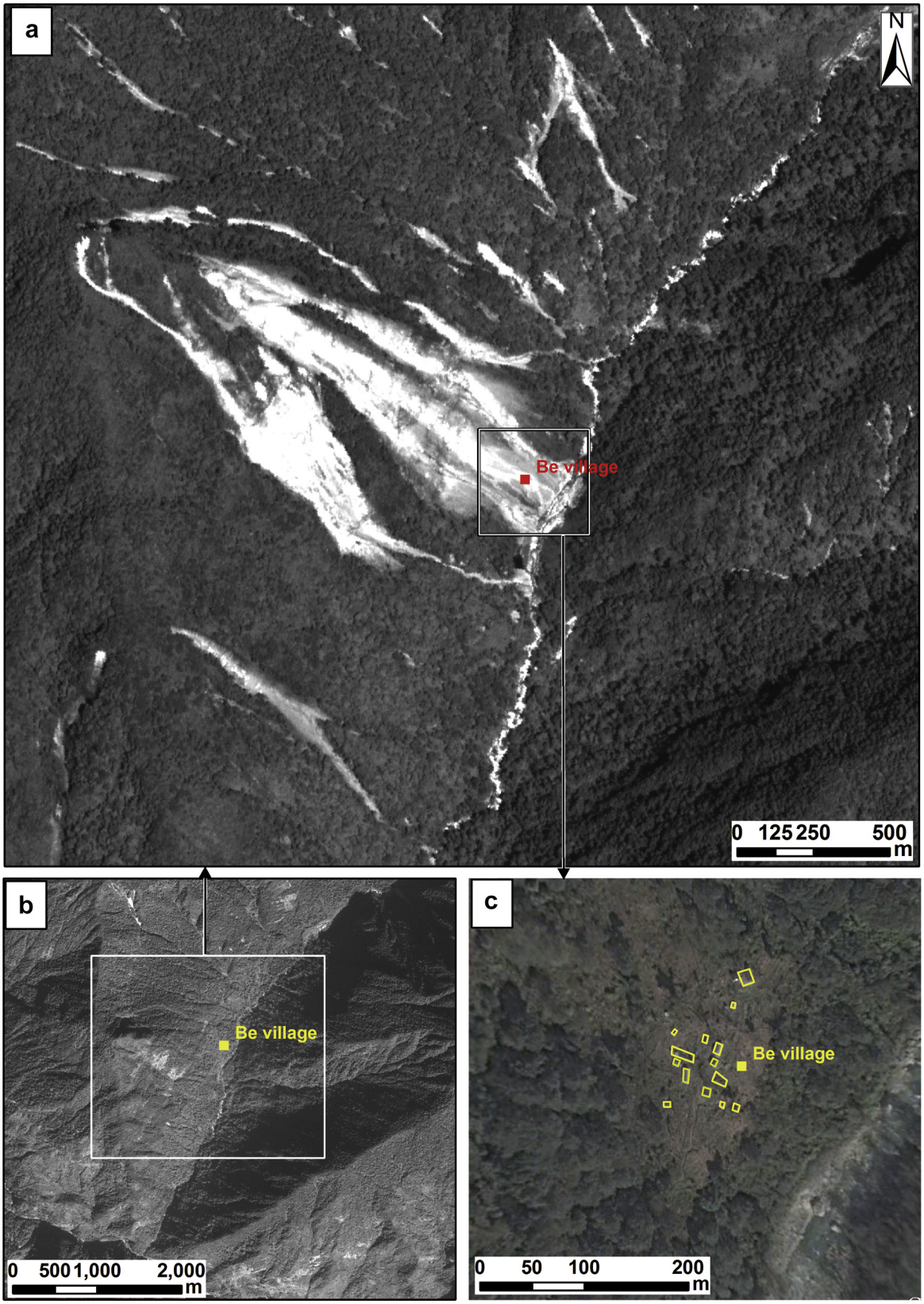

Figure 8. Be village landslide in north Sikkim. (a) Post-earthquake Cartosat-1 image, (b) pre-earthquake Cartosat-1 image, and (c) Google Earth image of 2010 showing location of houses (yellow outlines).

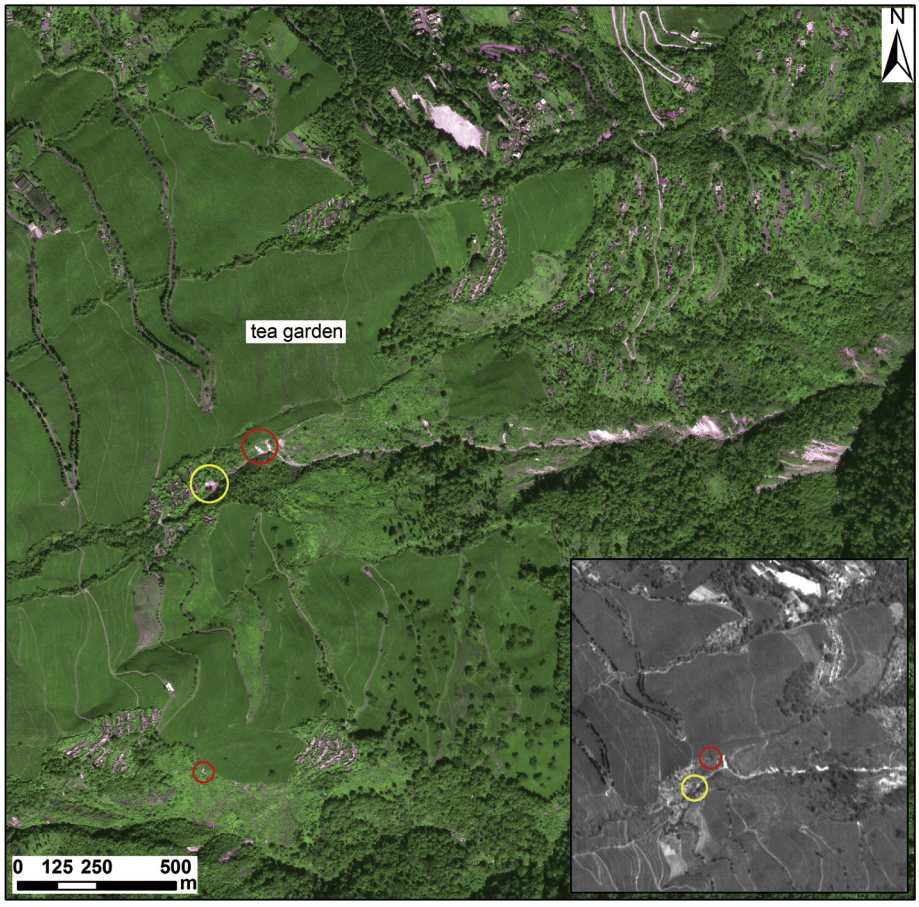

Figure 9. Post-earthquake natural colour composite (RGB = 432) of pansharpened GeoEye-1 image showing a tea garden in south Sikkim. Inset shows a pre-earthquake Cartosat-1 image of the same area. Peripheral part of the tea garden including the small settlements where workers mainly stay were affected by landslides (shown with yellow circle) triggered due to the earthquake. New landslides are highlighted with red circles.

3.1. Post-earthquake landslide inventory

The Sikkim Himalaya is susceptible to landslide occurrences (Mehrotra et al., 1996). Landslides cause exposure of fresh rocks and soils, and removal of vegetation. These effects can be seen clearly in the post-earthquake image in the form of high image brightness. Some other features such as barren land, roads and river sands also provide similar tone and could be incorrectly interpreted as landslides. Due to several developmental activities in this area, road cuttings can be erroneously interpreted as post-earthquake landslides since they also give as high brightness as landslides (Fig. 2). However, a careful analysis of the image tone in association with texture, shape and pattern can help accurate identification of landslides. Demarcation of landslides as polygons, though ideal, was avoided in this study since it was time consuming (Voigt et al., 2007). Therefore, landslide locations were marked as points. The points were placed in the zones of initiation of the landslides by using methods similar to those applied by Gorum et al. (2011) for the 2008 Wenchuan earthquake. Most of the landslides were of shallow translational nature, which could be interpreted so from their size and elongated shape. However, large rock falls and rock slides were also observed in this area. Large boulders detached from the vertical rock cliff and clearly seen in the GeoEye-1 image (38 cm) were identified as rock fall zones. Occurrence of rock falls and rock slides is typical after an earthquake (Jibson et al., 2006). Old landslides, reactivated due to the earthquake, were identified and mapped as new landslides in this study (Fig. 3). A total of 1196 new landslides were mapped using post-earthquake satellite images (Fig. 4).

3.2. Infrastructural damage

Several parts of Sikkim remained inaccessible for many days after the earthquake mainly due to the blockage of roads. It was possible to identify such areas using VHR images. Fig. 5 shows how a part of the road previously affected by a landslide was again affected by new landslide occurrences due to the earthquake. Areas such as Mangan and Chungthang, which are close to the earthquake epicentre, were severely affected and several roads were either destroyed or blocked by the debris (Fig. 6).

Another important infrastructure, which is of concern, is the two hydroelectric dams: one across Tista river and the other across Rangit river (tributary to Tista). No major damage was observed from the VHR images in the dam area except the occurrence of landslides in the reservoir catchment area (Fig. 7). These landslides will contribute sediments to the reservoir after the rainfall, resulting in enhancement of siltation-related problems. Apart from blocking roads, landslides are capable of blocking rivers (Dunning et al., 2007). In this analysis no such major blockages and creation of temporary reservoirs were observed except for a few minor ones upstream of Tolung Chu, a tributary of the Tista river.

3.3. Building damage

As per the news report, some buildings collapsed and several others developed cracks due to the earthquake. During the analysis of the VHR images of some of the major settlements in this area, we could not find any noticeable change. This could be due to

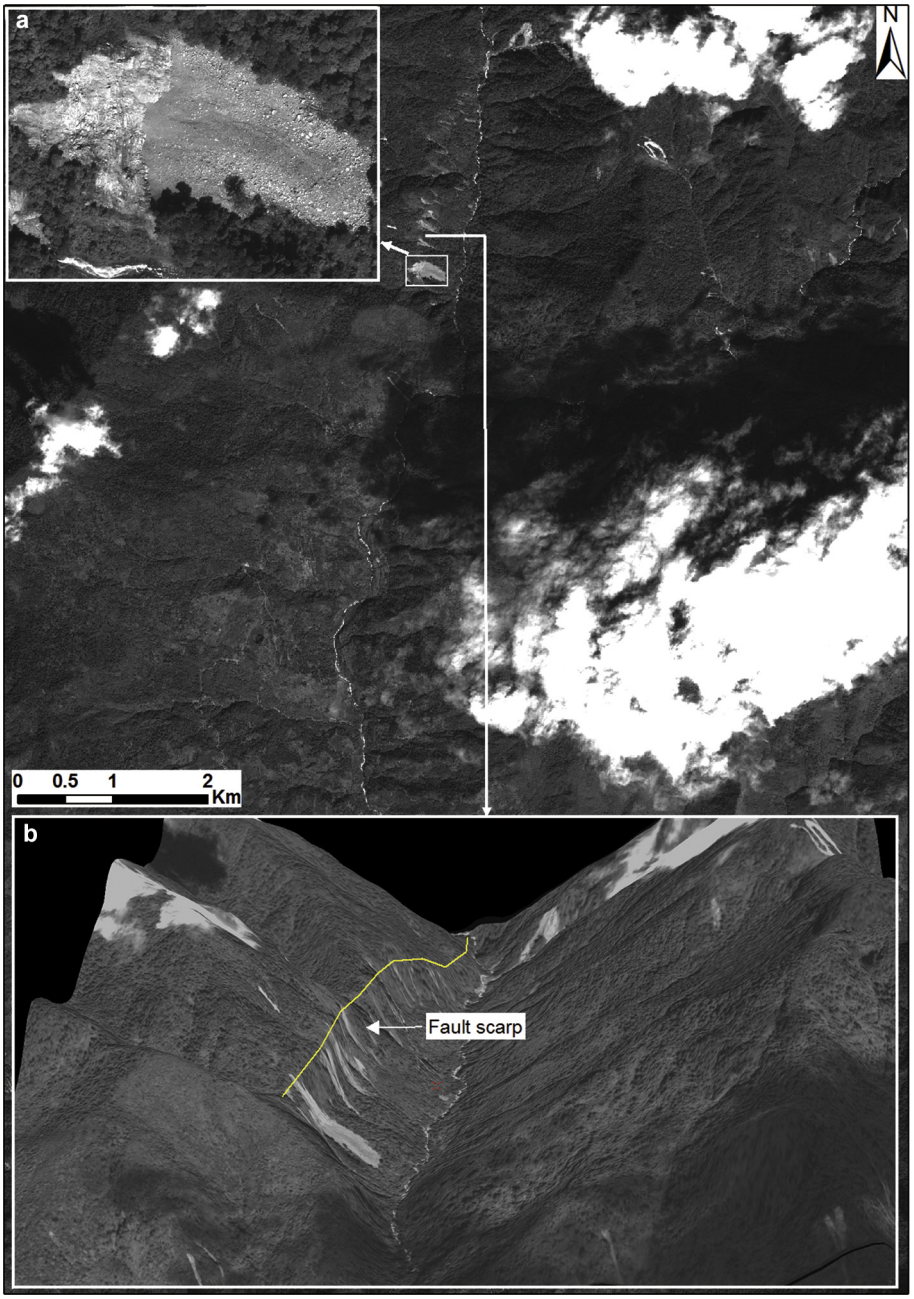

Figure 10. Post-earthquake panchromatic image of GeoEye-1. (a) shows a large rock fall. Source area of the rock fall as well as the debris could be seen clearly in the VHR image. (b) shows 3D perspective of the fault scarp with the yellow line marked on a prominent break-in-slope. Linear disposition of large rock falls along the scarp suggests reactivation of the fault.

the lack of sufficient image signatures of the damaged buildings. However, one village was completely destroyed by a large landslide in the upstream areas of Tolung Chu (river) (Fig. 8). A news report suggested that 120 people were missing from this village. Similarly, in the Chungthang area, a few buildings were also observed in the run out zones of the landslides, indicating a high possibility of damage.

3.4. Agricultural damage

Agricultural lands in steep Himalayan terrain are limited and precious. Some of these lands in southern Sikkim are well known for tea cultivation. Periphery of the tea gardens, which is mostly in the steep slopes were affected by landsliding (Fig. 9).

3.5. Geological assessment

High-magnitude earthquakes could cause reactivation of faults. Previously, stereoscopic interpretation of satellite images was used to demarcate fault scarps (Salvi, 1995). Fu et al. (2004) showed the usefulness of ASTER 3D images for mapping active faults associated with the 2003 Bam earthquake in Iran. Similarly, Chini et al. (2011) showed building damages and occurrence of landslides due to rupturing along a pre-existing fault scarp in an area west of Neelum river in Muzaffarabad, Pakistan after the 2005 Kashmir earthquake. Such disposition of landslides along a prominent lineament or fault scarp is one of the key criteria to identify locations of fault reactivation after the earthquake. In this area, along one of the N–S oriented scarp, alignment of large rock slides/falls was prominently

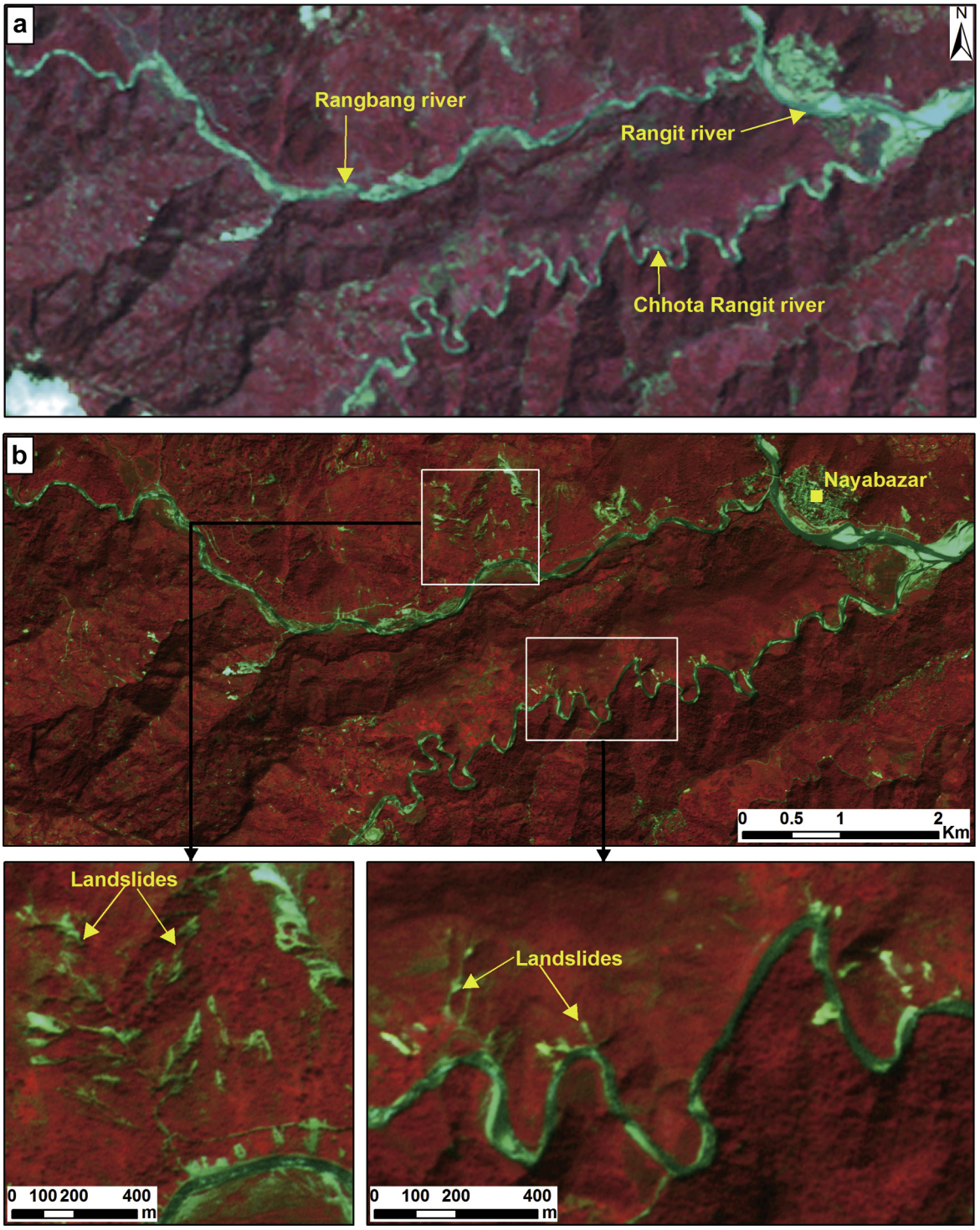

Figure 11. Landslides triggered along MCT in the Nayabazar area. (a) Landsat-5 TM image acquired six days before the earthquake shows minor presence of landslides, (b) Resourcesat-2 LISS IV Mx image showing several landslides triggered due to the earthquake along Rangbang and Chhota Rangit rivers.

observed during the stereoscopic interpretation of Cartosat-1 (Fig. 10). This type of evidence suggests reactivation of a fault. However, the movement across the lineament should be confirmed with other geophysical datasets.

Similarly, areas west of Nayabazar in the border between West Bengal and Sikkim states, witnessed occurrence of 113 new landslides after the earthquake (Fig. 11). These landslides occurred along the Rangbang and Chhota Rangit river valleys, which represents MCT on the surface. Linear disposition of these landslides along an existing fault suggests its reactivation due to the earthquake. Further in Lachen, Chungthang and Nadom areas, several landslides were triggered after the earthquake, in river valleys (e.g. Tolung Chu valley in Fig. 4) which coincides with the fault mapped by GSI (2000).

Areas close to the earthquake epicentre generally witness occurrence of numerous landslides. To verify this, we compared the

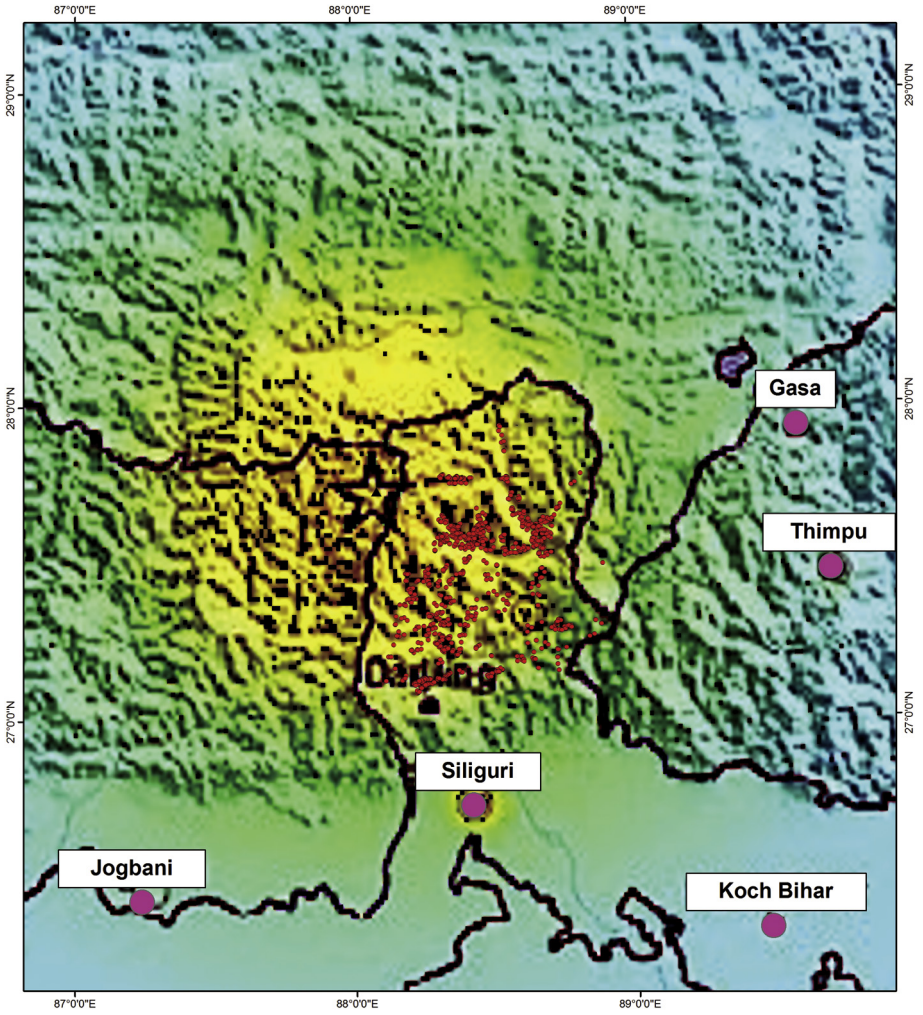

Figure 12. Landslide locations (red dots) shown on USGS shake map. Most of the landslides within the Sikkim area are confined to the yellow coloured (strong shaking) zone of the Sikkim earthquake.

shake map, which shows the strength of shaking due to the strong ground motion of an earthquake, with the event-based landslide inventory map prepared by us. Firstly, we georeferenced the shake map published by USGS (2011) and then plotted the landslide locations over it. The result showed a good match between the landslide locations and strong shaking areas of the Sikkim earthquake (Fig. 12). The gap in landslide locations in the Nepal–Sikkim border in west Sikkim and in the Sikkim–China border in north Sikkim, is due to the difficulty in identification of landslides, since, those areas are in the Kanchejunga peak zones, which are permanently snow covered.

4. Discussion

In this study, we mapped different types of landslides (rock slides, rock falls and debris slides) and showed their relationship with faults/thrusts. From the spatial relationship between landslides and faults, it is quite clear that some of the faults were reactivated due to the Sikkim earthquake. Recently, Ravi Kumar et al. (2012) also showed that several aftershocks in the Tolung Chu valley are aligned along the major lineaments, and therefore landslides in this valley can be attributed to rupturing along the major fault line. We have also shown the spatial distribution of landslides with respect to the shake map produced by USGS, which clearly shows that the maximum number of landslides occurred close to the earthquake epicentre. However, apart from the ground acceleration and geological structures (faults/thrusts), there are other factors such as slope, lithology and vegetation which also significantly contributed to the occurrence of co-seismic landslides. Recently, Ghosh et al. (2012), using 210 coseismic landslides identified through ground investigations, showed that landslides have positive spatial association with Gondwana sediments, metapelitic rocks of Daling Group and Chungthang gneiss. However, to the contrary, they observed that slope has no positive spatial relationship with landslides, which could be due to the mapping of landslides only along the roads. An investigation using the landslide inventory prepared by us may provide a better and meaningful spatial association between landslides and terrain factors. Finally, a careful analysis of these terrain factors will lead to a better seismogenic landslide hazard zonation of the Sikkim Himalayas.

5. Conclusions

This paper highlights the importance of VHR images in a disaster response situation. The main contribution of the paper is the rapid assessment of an area of 4105 km^2 in Sikkim using 123 images from eight satellites. Acquisition of satellite images under the coordinated effort of ICSMD was very helpful and data for the affected area were available in a short time, which helped in rapid damage assessment and quick dissemination of results. Preliminary results

highlighting the affected areas were hosted on 04 October 2011 in the NRSC website (www.nrsc.gov.in) for disseminating information to general public.

A total of 1196 new landslides were mapped in the Sikkim area. Mangan and Chungthang areas in North Sikkim were found to be severely affected due to landsliding. Be village, west of Mangan was completely destroyed by a large rock slide. Many roads along the Tista river and its tributaries, were either blocked or completely dislodged by landslides. Landslides were also mapped in the reservoir catchment areas which could cause siltation-related problems in the future.

3D visualisation coupled with detail information of the terrain provided by VHR images was helpful to identify location of rock falls along an escarpment suggesting reactivation of faults due to the earthquake. Linear disposition of landslides along existing faults also suggests their reactivation due to the earthquake. The event-based landslide inventory map prepared from VHR images matched well with the earthquake shake map of USGS.

Although results from the rapid assessment of Sikkim earthquake were presented in this paper, delay in the availability of cloud-free data after the earthquake by nine days delayed the extraction of immediate assessment results. Microwave data, although available immediately after the earthquake, could not be interpreted due to foreshortening and layover effects. This calls for development of new techniques for damage assessment using microwave data in rugged mountainous areas. Nevertheless, this paper presents a rapid and detailed assessment of earthquake damage in the vast and inaccessible areas in Sikkim, which otherwise would have been difficult and time consuming.

Acknowledgements

This paper is the outcome of the disaster support work carried out under the Decision Support Centre (DSC) activities of NRSC. We thank ICSMD for providing VHR satellite data for assessment of the earthquake-affected area. The support by Dr. V.K. Dadhwal, Director, NRSC and G. Behera, former Deputy Director, Remote Sensing and GIS Applications Area, NRSC is duly acknowledged. The last author is thankful to ICSMD for identifying him as project manager for Charter call 372 (Earthquake in northeast India). The authors thank Rynn M. Lamb, disaster response coordinator, USGS and Dr. N. Aparna, NRSC and Dr. R. Nagaraja, Head, NDC for quick dissemination of satellite data for analysis.

References

Arciniegas, G.A., Bijker, W., Kerle, N., Tolpekin, V.A., 2007. Coherence- and amplitude-based analysis of seismogenic damage in Bam, Iran, using ENVISAT ASAR data. IEEE Transactions on Geoscience and Remote Sensing 45, 1571–1581.

Chini, M., Cinti, F.R., Stramondo, S., 2011. Co-seismic surface effects from very high resolution panchromatic images: the case of the 2005 Kashmir (Pakistan) earthquake. Natural Hazards and Earth System Sciences 11, 931–943.

Di, B., et al., 2010. Quantifying the spatial distribution of soil mass wasting processes after the 2008 earthquake in Wenchuan, China: a case study of the Longmenshan area. Remote Sensing of Environment 114, 761–771.

Dunning, S.A., Mitchell, W.A., Rosser, N.J., Petley, D.N., 2007. The Hattian Bala rock avalanche and associated landslides triggered by the Kashmir earthquake of 8 October 2005. Engineering Geology 93, 130–144.

Fu, B., Ninomiya, Y., Lei, X., Toda, S., Awata, Y., 2004. Mapping active fault associated with the 2003 Mw 6.6 Bam (SE Iran) earthquake with ASTER 3D images. Remote Sensing of Environment 92, 153–157.

Gamba, P., Dell'Acqua, F., Trianni, G., 2007. Rapid damage detection in the Bam area using multitemporal SAR and exploiting ancillary data. IEEE Transactions on Geoscience and Remote Sensing 45, 1582–1589.

Ghosh, S., Chakraborty, I., Bhattacharya, D., Bora, A., Kumar, A., 2012. Generating field-based inventory of earthquake-induced landslides in the Himalayas-an aftermath of the 18 September 2011 Sikkim earthquake. Indian Journal of Geosciences 66, 27–38.

Ghosh, S., Gunther, A., Carranza, E.J.M., van Westen, C.J., Jetten, V.G., 2010. Rock slope instability assessment using spatially distributed structural orientation data in Darjeeling Himalaya (India). Earth Surface Processes and Landforms 35, 1773–1792.

Gorum, T., et al., 2011. Distribution pattern of earthquake-induced landslides triggered by the 12 May 2008 Wenchuan earthquake. Geomorphology 133, 152–167.

GSI, 2000. Seismotectonic Atlas of India and Its Environs. Geological Survey of India, Calcutta, India.

Jibson, R.W., Harp, E.L., Schulz, W., Keefer, D.K., 2006. Large rock avalanches triggered by the M 7.9 Denali Fault, Alaska, earthquake of 3 November 2002. Engineering Geology 83, 144–160.

Kayal, J.R., 2001. Microearthquake activity in some parts of the Himalayas and the tectonic model. Tectonophysics 339, 331–351.

Kumar, P., et al., 2007. The rapid drift of the Indian tectonic plate. Nature 449, 894–897.

Lodhi, M.A., 2011. Earthquake-induced landslide mapping in the western Himalayas using medium resolution ASTER imagery. International Journal of Remote Sensing 32, 5331–5346.

Lodhi, M.A., 2013. Multisensor imagery analysis for mapping and assessment of 12 January 2010 earthquake-induced building damage in Port-au-Prince, Haiti. International Journal of Remote Sensing 34, 451–467.

Mahajan, A.K., Gupta, V., Thakur, V.C., 2012. Macroseismic field observations of 18 September 2011 Sikkim earthquake. Natural Hazards 63, 589–603.

Mehrotra, G.S., Sarkar, S., Kanungo, D.P., Mahadevaiah, K., 1996. Terrain analysis and spatial assessment of landslide hazards in parts of Sikkim Himalaya. Journal of the Geological Society of India 47, 491–498.

Metternicht, G., Hurni, L., Gogu, R., 2005. Remote sensing of landslides: an analysis of the potential contribution to geo-spatial systems for hazard assessment in mountainous environments. Remote Sensing of Environment 98, 284–303.

Ravi Kumar, M., Hazarika, P., Srihari Prasad, G., Singh, A., Saha, S., 2012. Tectonic implications of the September 2011 Sikkim earthquake and its aftershocks. Current Science 102, 788–792.

Ray, P.K.C., et al., 2009. Analysis of seismicity-induced landslides due to the 8 October 2005 earthquake in Kashmir Himalaya. Current Science 97, 1742–1755.

Saha, D., 2013. Lesser Himalayan sequences in Eastern Himalaya and their deformation: implications for Paleoproterozoic tectonic activity along the northern margin of India. Geoscience Frontiers 4, 289–304.

Salvi, S., 1995. Analysis and interpretation of Landsat synthetic stereo pair for the detection of active fault zones in the Abruzzi region (Central Italy). Remote Sensing of Environment 53, 153–163.

Shen, J., Wang, Y., Li, Y., 2011. Characteristics of the Late Quarternary right-lateral strike-slip movement of Bolokenu-Aqikekuduk fault in northern Tianshan Mountains, NW China. Geoscience Frontiers 2, 519–527.

Stumpf, A., Kerle, N., 2011. Object-oriented mapping of landslides using random forests. Remote Sensing of Environment 115, 2564–2577.

Tralli, D.M., Blom, R.G., Zlotnicki, V., Donnellan, A., Evans, D.L., 2005. Satellite remote sensing of earthquake, volcano, flood, landslide and coastal inundation hazards. ISPRS Journal of Photogrammetry and Remove Sensing 59, 185–198.

USGS, 2011. Shake Map: India-Nepal Border Region. http://earthquake.usgs.gov/earthquakes/shakemap/global/shape/c0005wg6/#Instrumental_Intensity.

Vinod Kumar, K., Martha, T.R., Roy, P.S., 2006. Mapping damage in the Jammu and Kashmir caused by 8 October 2005 Mw 7.3 earthquake from the Cartosat–1 and Resourcesat–1 imagery. International Journal of Remote Sensing 27, 4449–4459.

Voigt, S., et al., 2007. Satellite image analysis for disaster and crisis-management support. IEEE Transactions on Geoscience and Remote Sensing 45, 1520–1528.

Wang, F., et al., 2009. Preliminary investigation of some large landslides triggered by the 2008 Wenchuan earthquake, Sichuan Province, China. Landslides 6, 47–54.

Xu, C., Xu, X., Yao, X., Dai, F., 2013a. Three (nearly) complete inventories of landslides triggered by the May 12, 2008 Wenchuan Mw 7.9 earthquake of China and their spatial distribution statistical analysis. Landslides 11 (3), 441–461. http://dx.doi.org/10.1007/s10346-013-0404-6.

Xu, C., Xu, X., Yu, G., 2013b. Landslides triggered by slipping-fault generated earthquake on a plateau: an example of the 14 April 2010, Ms 7.1, Yushu, China earthquake. Landslides 10, 421–431.